Highly efficient cellular uptake of a cell-penetrating peptide (CPP) derived from the capsid protein of porcine circovirus type 2

Received for publication, July 19, 2018, and in revised form, August 9, 2018 Published, Papers in Press, August 14, 2018, DOI 10.1074/jbc.RA118.004823

Wanting Yu[‡§], Yang Zhan[‡§], Boxin Xue[¶], Yanpeng Dong[‖], Yanfeng Wang[**], Ping Jiang[‖], Aibing Wang[‡§], Yujie Sun[¶1], and Yi Yang[‡§2]

From the [‡]Key Laboratory of Animal Vaccine and Protein Engineering and [§]Laboratory of Functional Proteomics (LFP) and Research Center of Reverse Vaccinology (RCRV), College of Veterinary Medicine, Hunan Agricultural University, Changsha 410128, China, [¶]State Key Laboratory of Membrane Biology, Biodynamic Optical Imaging Center (BIOPIC), School of Life Sciences, Peking University, Beijing 100871, China, [‖]College of Veterinary Medicine, Nanjing Agricultural University, Nanjing 210095, China, and [**]Tsinghua-Peking Joint Center for Life Science, Tsinghua University, Beijing 100084, China

Edited by Charles E. Samuel

Porcine circovirus type 2 (PCV2) is one of the smallest, nonenveloped, single-stranded DNA viruses. The PCV2 capsid protein (Cap) is the sole viral structural protein and main antigenic determinant. Previous sequence analysis has revealed that the N terminus of the PCV2 Cap contains a nuclear localization signal (NLS) enriched in positively charged residues. Here, we report that PCV2's NLS can function as a cell-penetrating peptide (CPP). We observed that this NLS can carry macromolecules, *e.g.* enhanced GFP (EGFP), into cells when they are fused to the NLS, indicating that it can function as a CPP, similar to the classical CPP derived from HIV type 1 transactivator of transcription protein (HIV TAT). We also found that the first 17 residues of the NLS (NLS-A) have a key role in cellular uptake. In addition to entering cells via multiple endocytic processes, NLS-A was also rapidly internalized via direct translocation enabled by increased membrane permeability and was evenly distributed throughout cells when its concentration in cell cultures was ≥10 μM. Of note, cellular NLS-A uptake was ~10 times more efficient than that of HIV TAT. We inferred that the externalized NLS of the PCV2 Cap may accumulate to a high concentration (≥10 μM) at a local membrane area, increasing membrane permeability to facilitate viral entry into the cell to release its genome into a viral DNA reproduction center. We conclude that NLS-A has potential as a versatile vehicle for shuttling foreign molecules into cells, including pharmaceuticals for therapeutic interventions.

Porcine circovirus (PCV),[3] one of the smallest animal viruses, belongs to the *Circovirus* genus in the family Circoviridae (1) and is a nonenveloped, single-stranded, and circular DNA virus. There are three genotypes of which PCV type 2 (PCV2) has been associated with various diseases, collectively termed porcine circovirus 2–associated diseases (2), whereas PCV type 1 (PCV1) is nonpathogenic for swine (3). In addition, PCV type 3 (PCV3), a newly emerging circovirus, was reported in 2016, and its pathogenicity has yet to be determined (4, 5).

Currently, PCV2 is regarded as one of the world's most important swine pathogens, causing huge economic losses. The PCV2 genome contains two main open reading frames (ORFs). Of those, ORF1 encodes two replication-related proteins (Rep and Rep′), both of which are indispensable to virus replication, whereas ORF2 encodes capsid protein (Cap), the sole structural protein of this virus, capable of self-assembly into virus-like particles *in vivo* or *in vitro*. The NH_2 terminus of the Cap, consisting of 41 residues, is the nuclear localization signal (NLS), based on subcellular localizations of various PCV2 Cap mutants, including truncated Cap (without the NLS) that was not detected in the nucleus (6). The NLS is enriched with positively charged residues, often present in other NLS-containing proteins. A unique signature of the NLS of the PCV Cap is an arginine-rich stretch. Interestingly, the NLS of Caps derived from other circovirus species (*e.g.* those affecting ducks or dogs) also contains substantial arginine residues. However, functions of these arginine residues in the NLS have not yet been confirmed. The NLS may be proximal to the icosahedral 5-fold axis of the PCV2 capsid and be involved in viral DNA packaging (7). Therefore, the NLS might not be exposed on the capsid surface in a mature virion, although it might externalize in the metastable capsid, induced by various cellular or environmental fac-

This work was supported by the National Nature Science Foundation of China (Grants 31270819, 31571432, and 21573013), the National Key Research and Development Program of China (Grant 2017YFA0505300), the Talent Input Project of Hunan Agricultural University (Grant 540490317006), and the Hunan Provincial Key Laboratory of Protein Engineering in Animal Vaccines (Grant 2017TP1014). The authors declare that they have no conflicts of interest with the contents of this article.

This article contains Figs. S1–S5.

[1] To whom correspondence may be addressed. Tel.: 86-010-62744060; Fax: 86-010-62744060; E-mail: sun_yujie@pku.edu.cn.

[2] To whom correspondence may be addressed: Research Center of Reverse Vaccinology (RCRV) and Laboratory of Functional Proteomics (LFP), College of Veterinary Medicine, Hunan Agricultural University, Changsha 410128, China. Tel.: 86-731-84635276; Fax: 86-731-84635276; E-mail: yiyang@hunau.edu.cn.

[3] The abbreviations used are: PCV, porcine circovirus; Cap, capsid protein; NLS, nuclear localization signal; CPP, cell-penetrating peptide; EGFP, enhanced GFP; HIV TAT, HIV type 1 transactivator of transcription protein; CRAC, cholesterol recognition amino acid consensus; PI, propidium iodide; GUV, giant unilamellar vesicle; RFP, red fluorescent protein; HS, heparan sulfate; HSPG, heparan sulfate proteoglycan; CME, clathrin-mediated endocytosis; PK, porcine kidney epithelial; DiI, 1,1″-dioctadecyl-3,3,3″,3″-tetramethylindocarbocyanine perchlorate; EMCCD, electron-multiplying charge-coupled device.

tors during virus entry into host cells. However, roles of the NLS in PCV2 entry into host cells are unknown.

The NLS of adenovirus E1A can deliver macromolecules into a nucleus by interacting with the nuclear pore complex in nondividing cells, which can further be recognized by nuclear import transporters (8, 9). Furthermore, NLS peptides derived from simian virus 40 (KKKRKV) and nucleoplasmin (KRPAAIKKAGQAKKKK) may function as cell-penetrating peptides (CPPs), delivering foreign proteins into cells, although both peptides have poor efficiencies for cellular uptake with their functional motifs rich in lysine residues (10).

CPP, a powerful transport vector for delivery of various cargoes through cell membranes, was first described in 1988 and is derived from a peptide of HIV type 1 transactivator of transcription protein (HIV TAT) (11). In 1997, Vivès *et al.* (12) identified a minimal sequence with 11 residues from HIV TAT that penetrated cell membranes and entered cells. A few years later, Derossi, D. *et al.* (13) discovered another CPP, a 16-residue peptide of penetratin (pAntp) derived from the amphiphilic *Drosophila* Antennapedia homeodomain. Over the past 20 years, >100 peptides, ranging from 5 to 40 residues, have been reported to penetrate various cell membranes and carry biologically active molecules, cargoes, and compounds into cells (14). Among these CPPs, the HIV TAT–based delivery system has been extensively studied in cultured cells and organs (15). For example, by bioconjugation with imaging agents, HIV TAT can be used for intracellular imaging (16, 17), whereas by covalent attachment of oligonucleotides, HIV TAT can function as a vehicle to deliver foreign DNA into cells (18).

Although CPPs are efficient intracellular delivery systems, they have limitations in practical applications. First, HIV TAT was reported to move out of cells, thereby reducing intracellular concentrations of HIV TAT–attached compounds (17). Second, HIV TAT and some CPPs might be trapped in endosomes and degraded during endosome maturation (19, 20). Third, toxic side effects usually occur with HIV TAT–mediated delivery (12, 15, 21).

Elucidating mechanisms of CPP cellular uptake should facilitate development of novel delivery vectors. It was reported that CPPs enter cells by either directly penetrating cell membranes for internalization or endocytosis-mediated translocation (22–24). In addition, energy-dependent macropinocytosis is considered a primary endocytosis pathway responsible for CPP-mediated intracellular delivery of various proteins (25–28). In that regard, dimeric HIV TAT had a crucial role in the subsequent endosomal escape of these foreign proteins into the cytoplasm (27). Regardless, precise mechanisms regarding cellular uptake of various CPPs remain to be determined.

In this study, NLS derived from the PCV2 Cap carried foreign protein into various cell lines. Furthermore, roles of two positively charged segments (NLS-A and -B) among the NLS were investigated: NLS-A, but not -B, may function as a novel CPP capable of entering cells. In addition, mechanisms of NLS-A cellular uptake at different concentrations were also studied by live-imaging microscopy because fixation reagents might lead to artificial redistribution due to the positively charged nature of the CPP (29). Finally, we raised a possible model in which the NLS of the PCV Cap may have essential roles in interactions of virus–host cells and release of a viral genome into a replication site via increased membrane permeability.

Results

The arginine-rich NLS was a signature of PCV Caps and present in other Circoviridae

The NLS was strictly conserved and enriched with arginine residues within Caps of both genotypes of PCV1 and PCV2 except for 2 extra residues (^{33}AF^{34}) in the NLS of the PCV1 Caps (Fig. 1*A*). Based on secondary structure analysis, the NLS of the PCV2 Cap was composed of two stretches (NLS-A and -B) separated by an α-helix (30), although this helix was absent in the PCV3 Cap (Fig. 1*A*). In PCV2, NLS-A contained 9 arginine residues, whereas NLS-B had 8 arginines and 1 lysine residue (Fig. 1, *A* and *C*). Furthermore, NLS derived from various circovirus species all had a signature motif rich in arginine residues (Fig. 1*B*). In addition, there was a well known and conserved motif of the cholesterol recognition amino acid consensus (CRAC) in PCV2 Caps (Fig. 1*C*). The CRAC motif, comprising -(L/V)X_{1-5}YX_{1-5}(R/K)- where X_{1-5} represents 1–5 residues of any amino acid at the position(s) (31), was only in NLS-B of PCV2 Caps, but not in PCV1, due to insertion of 2 residues in NLS-B (Fig. 1*A*).

The NLS of the PCV2 Cap carried foreign protein into various cells lines

To determine whether the arginine-rich NLS of the PCV2 Cap can carry foreign protein across cell membranes and enter cells *in vitro*, porcine kidney epithelial (PK15) (Fig. 2, *A–C*) or Sf9 cells (Fig. 2, *D–F*) were incubated with purified NLS-fused EGFP (NLS–EGFP) or EGFP (Fig. S1), respectively. The NLS–EGFP entered both cell lines (Fig. 2, *A* and *D*, *left panels*). In contrast, the fluorescence in EGFP-treated cells was significantly low (Fig. 2, *A* and *D*, *middle panels*). Flow cytometry analysis demonstrated that both PK15 cells and Sf9 cells incubated with NLS–EGFP had a significantly increased number of cells with intracellular fluorescence (Fig. 2, *B* and *E*) and higher mean fluorescence intensity (Fig. 2, *C* and *F*) compared with PK15 cells or Sf9 cells incubated with EGFP or the controls.

NLS-A, but not NLS-B, functioned as a CPP

Both NLS-A and -B are rich in positively charged residues and form two independent stretches divided by an α-helix (30) (Fig. 1*A*). Numbers of positively charged residues within each were comparable with two known CPPs (HIV TAT and polyarginine Arg_8) (Fig. 1*C*). We hypothesized that both NLS-A and -B may function as CPPs. To test this hypothesis, both peptides were synthesized, conjugated with FITC, and incubated with PK15 cells. NLS-A (Fig. 3*A*, *upper row*) entered PK15 cells, whereas NLS-B failed to enter cells (Fig. 3*A*, *middle row*). Flow cytometry analysis demonstrated that PK15 cells incubated with NLS-A had a significantly higher percentage of cells with intracellular fluorescence (Fig. 3*B*) and higher mean fluorescence intensity (Fig. 3*C*) than PK15 cells incubated with NLS-B or the control. In addition, besides PK15, both NLS-A and HIV TAT also entered HeLa and NIH3T3 cells (Fig. 4*A*).

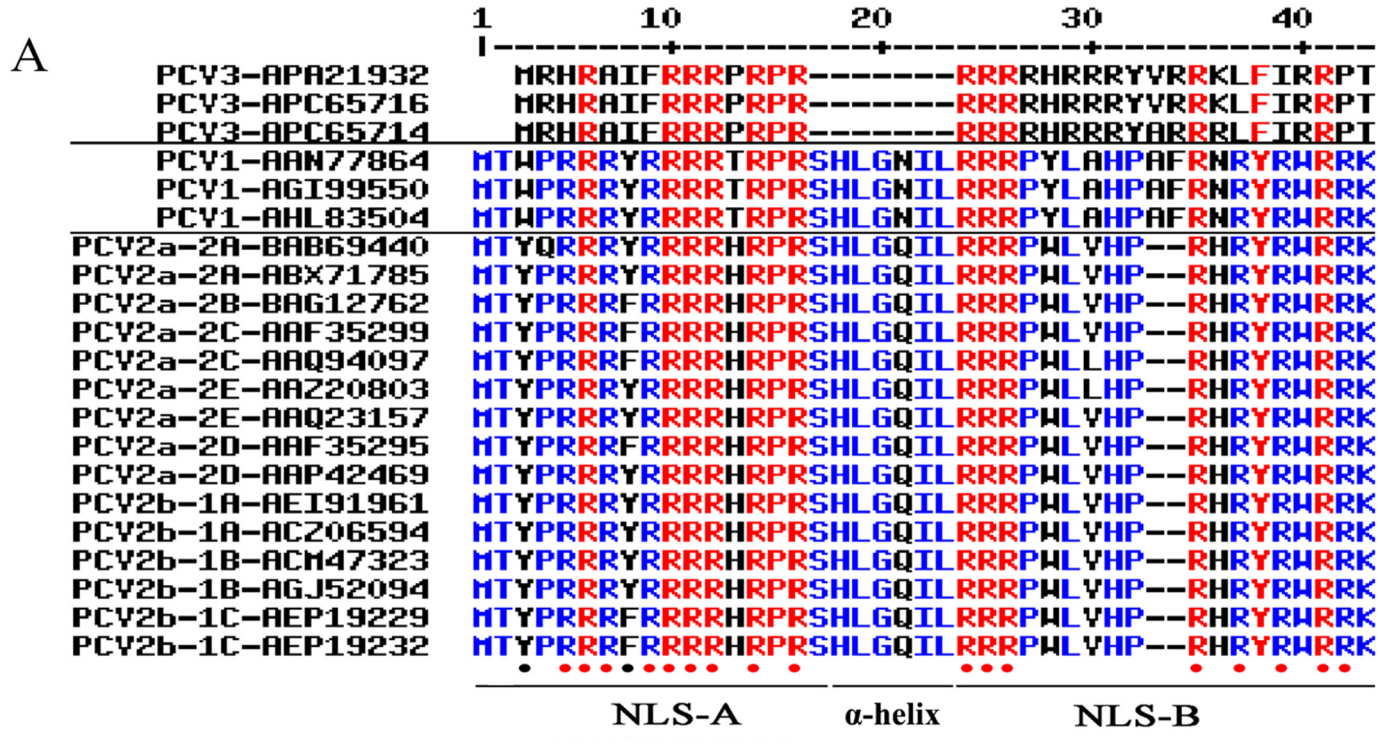

B

Circoviridae	Amino acid sequences of nuclear localization signals	UniProtKB ID
Porcine circovirus type 2 (PCV2)	RRRRHRPRSHLGQILRRRPWLVHPRHRYRWRRK	O56129
Porcine circovirus type 1 (PCV1)	RRRRTRPRSHLGNILRRRPYLAHPAFRNRYRWRRK	Q80QL5
Goose circovirus (GoCV)	RARPRSLYSRRRRATNRRRRYRRRRLHIGRIRSK	Q91EK1
Canary circovirus (CaCV)	ARRRRPLAPRRRRWRRRYWXRRRRIPANRRGHRT	Q8QME6
Chicken anemia virus (CAV)	RRPRGRFYSFRRGRWHHLKRLRRRYKFRHRRRQRYRRRAFRK	Q99153
Beak and feather disease virus (BFDV)	RRRYARPYRRRHIRRYRRRRRHFRRRRFTT	Q9YUC8
Duck circovirus (DuCV)	RRSTYRRAYRARRRRRGLRRRLRRRRLRIGRPRRR	A3FEQ4

C

TAT	YGRKKRRQRRR
R_8	RRRRRRRRR
NLS-A	MTYPRRRFRRRRHRPRS
NLS-B	QILRRRPWLVHPRHRYRWRRK
	V x x x x x Y x x R

Figure 1. Comparative sequence alignments of amino acid residues. *A*, primary structure alignment of the NLSs of PCV Caps. The NLS sequences from 21 PCV isolates collected from GenBank™ were aligned. The *right column* shows the genotype, subtype, and GenBank accession number of each sequence. *Red* indicates strictly conserved residues among all genotypes. A *hyphen* ("-") stands for a gap in the alignment. *B*, primary structure alignment of these NLSs of the Caps derived from six species of circovirus (UniProt protein IDs are indicated in the *right column*). Arginine is labeled in *red*. *C*, a comparison of NLS-A and -B with two known CPPs. Arginine is labeled in *red*. Note that a conserved CRAC motif (V*XXXXXYXX*R) was found in NLS-B.

Flow cytometry analysis (Fig. 4*B*) was consistent with the above confocal imaging result.

Concentration-dependent distribution and cellular uptake of NLS-A in cells

There was a punctate distribution pattern of NLS-A in cells after peptide internalization irrespective of peptide concentration in culture (Fig. 5*A*). Therefore, NLS-A may enter cells via endocytosis and localize within vesicles. However, an even distribution of the NLS-A throughout the cell cytoplasm, along with the punctate pattern, was also observed when peptide concentration in culture was ≥10 μM (Fig. 5*A*), implying a possible alternative concentration-dependent entry mechanism of NLS-A. In addition, flow cytometry analysis demonstrated that cellular uptake of NLS-A increased with elevated concentrations of this peptide in cell culture (Fig. 5, *B* and *C*). To exclude extracellular fluorescence (*e.g.* membrane surface–associated NLS-A), PK15 cells incubated with peptides or proteins were always treated with trypsin at 37 °C for 2 min (see "Materials and methods") before flow cytometry analysis (because NLS-A was sensitive to trypsinization; Fig. S2). In previous reports, CPPs had variable cytotoxicity at high concentration (12, 15, 21); accordingly, we also tested the cytotoxicity of NLS-A. Cells were treated with high concentration of NLS-A (40 μM) for 30 min followed by propidium iodide (PI) staining. As shown in Fig. 5*D* and Fig. S3, >90% of the cells were viable with incuba-

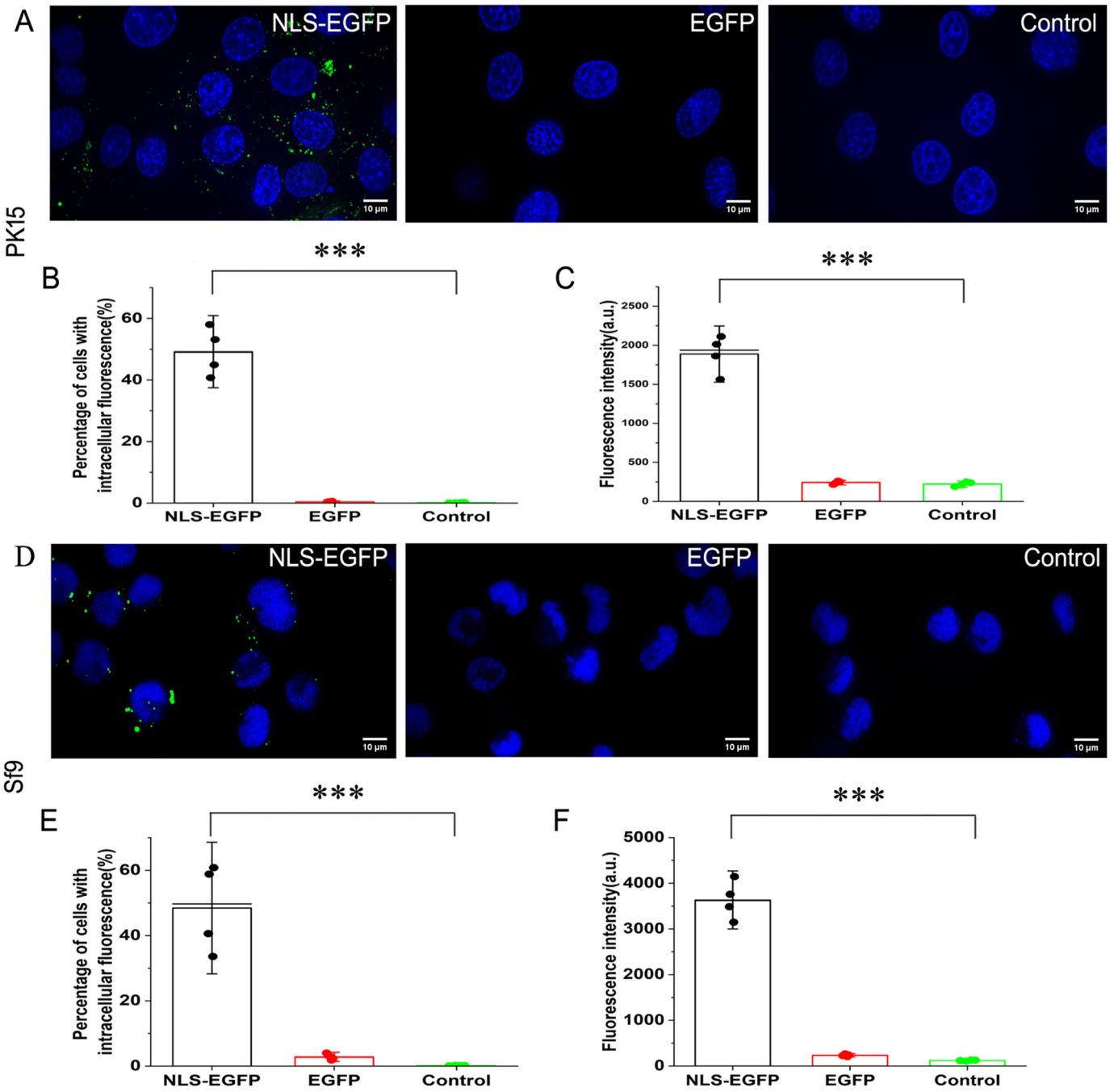

Figure 2. NLS–EGFP recombinant proteins entered both PK15 cells and Sf9 cells. *A*, PK15 cells were incubated with 4 μg/ml NLS–EGFP (*left*) or EGFP (*middle*) for 1 h and washed three times with PBS before imaging with a dual-channel confocal laser-scanning microscope (Nikon TiE). A third test with Opti-MEM incubation only was used as a treatment control (*right*). *Green* indicates EGFP signal in the cells, and cell nuclei (*blue*) are indicated by Hoechst. *B*, bar graph summarizing the percentage of the PK15 cells with intracellular fluorescence under the above three incubation treatments ($n = 4$; *error bars* represent S.D.; ***, $p < 0.001$). *C*, bar graph summarizing fluorescence intensity of the PK15 cells under the above three incubation treatments ($n = 4$; *error bars* represent S.D.; ***, $p < 0.001$). *D*, Sf9 cells were incubated with NLS–EGFP (*left*) or EGFP (*middle*) for 1 h and washed three times with PBS before imaging with a dual-channel confocal laser-scanning microscope (Nikon TiE). Another test with Opti-MEM incubation only was used as a treatment control (*right*). *Green* indicates EGFP signal in the cells, and cell nuclei (*blue*) are indicated by Hoechst. *E*, bar graph summarizing the percentage of the Sf9 cells with intracellular fluorescence under the above three incubation treatments ($n = 4$; *error bars* represent S.D.; ***, $p < 0.001$). *F*, bar graph summarizing fluorescence intensity of the Sf9 cells under the above three incubation treatments ($n = 4$; error bars represent S.D.; ***, $p < 0.001$). All *scale bars* represent 10 μm. *a.u.*, arbitrary units.

tion of NLS-A, even at a high concentration of 40 μM. Furthermore, we compared the cytotoxicity of NLS-A and HIV TAT upon PK15 cells at various concentrations. More than 95% of PK15 cells were viable under incubation of both CPPs that were lower than 20 μM (Fig. S3).

The NLS-A increased membrane permeability for cellular uptake

As suggested above in Fig. 5, the entry mechanism of NLS-A might be concentration-dependent. To further dissect the scenario, we monitored the NLS-A entry process by time-lapse

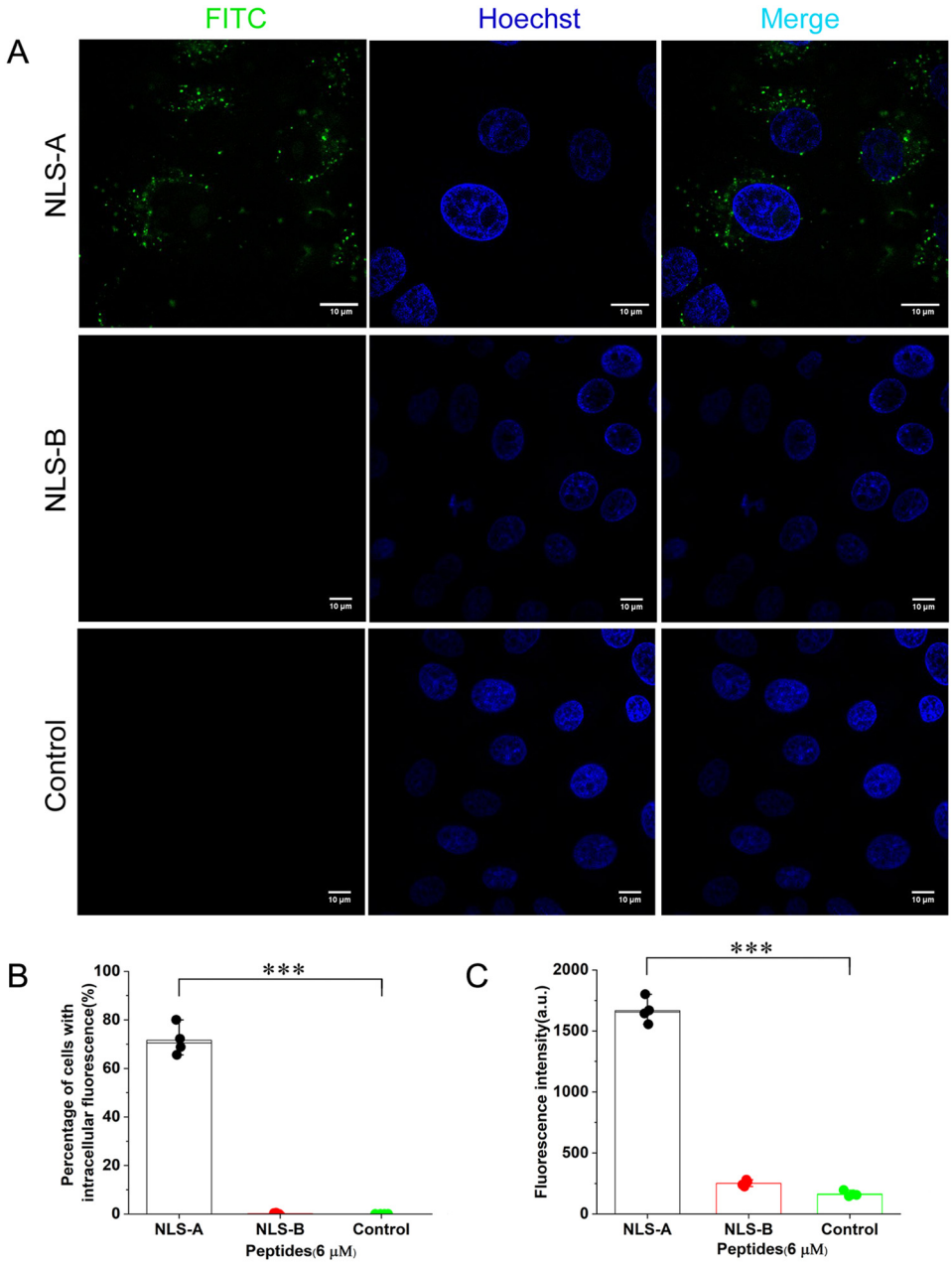

Figure 3. FITC-conjugated NLS-A entered PK15 cells. *A*, PK15 cells were incubated with 6 μM FITC-conjugated NLS-A (*upper row*) or 6 μM FITC-conjugated NLS-B (*middle row*) for 30 min and washed three times with PBS before imaging with a dual-channel confocal laser-scanning microscope (Nikon TiE). A third test with Opti-MEM incubation only was used as a treatment control (*bottom row*). Green indicates FITC signal in the cells, and cell nuclei (*blue*) are indicated by Hoechst. *B*, bar graph summarizing the percentage of the PK15 cells with FITC fluorescence under the above three incubation treatments ($n = 4$; *error bars* represent S.D.; ***, $p < 0.001$). *C*, bar graph summarizing fluorescence intensity of the PK15 cells under the above three incubation treatments ($n = 4$; *error bars* represent S.D.; ***, $p < 0.001$). All *scale bars* represent 10 μm. *a.u.*, arbitrary units.

confocal microscopy at high concentrations (40 μM). The increasing intracellular fluorescence signal was recorded every 5 s after the addition of peptide to cell culture (Fig. 6*A*), and the quantified intracellular mean fluorescence intensity was plotted against time (Fig. 6*B*). The rapid cellular uptake and even distribution of NLS-A suggested that the peptide may enter cells either through a receptor-independent pathway or by directly penetrating the cell membranes at high concentrations. To test whether NLS-A induced membrane permeability, we mixed NLS-A with giant unilamellar vesicles (GUVs) with encapsulated fluorescent dye (atto565) and monitored the GUVs with confocal microscopy. Fluorescence (red) within the GUVs turned green after NLS-A was mixed with the GUVs (Fig. 6, *C* and *D*), demonstrating the entry of NLS-A into the GUVs; in addition, the dye (red) in the GUVs also leaked out from the vesicles into the buffer. This result strongly indicated that NLS-A increased the permeability of the membrane and led to the equilibration of NLS-A and the atto565 dye across membranes (Fig. 6*D*). However, in the presence of FITC alone (Fig. 6*E*) or in the absence of NLS-A (Fig. 6*C*), the atto565 dye within the GUVs was quite stable. Statistical analysis also demonstrated that the ratio of GUVs containing green dye in the

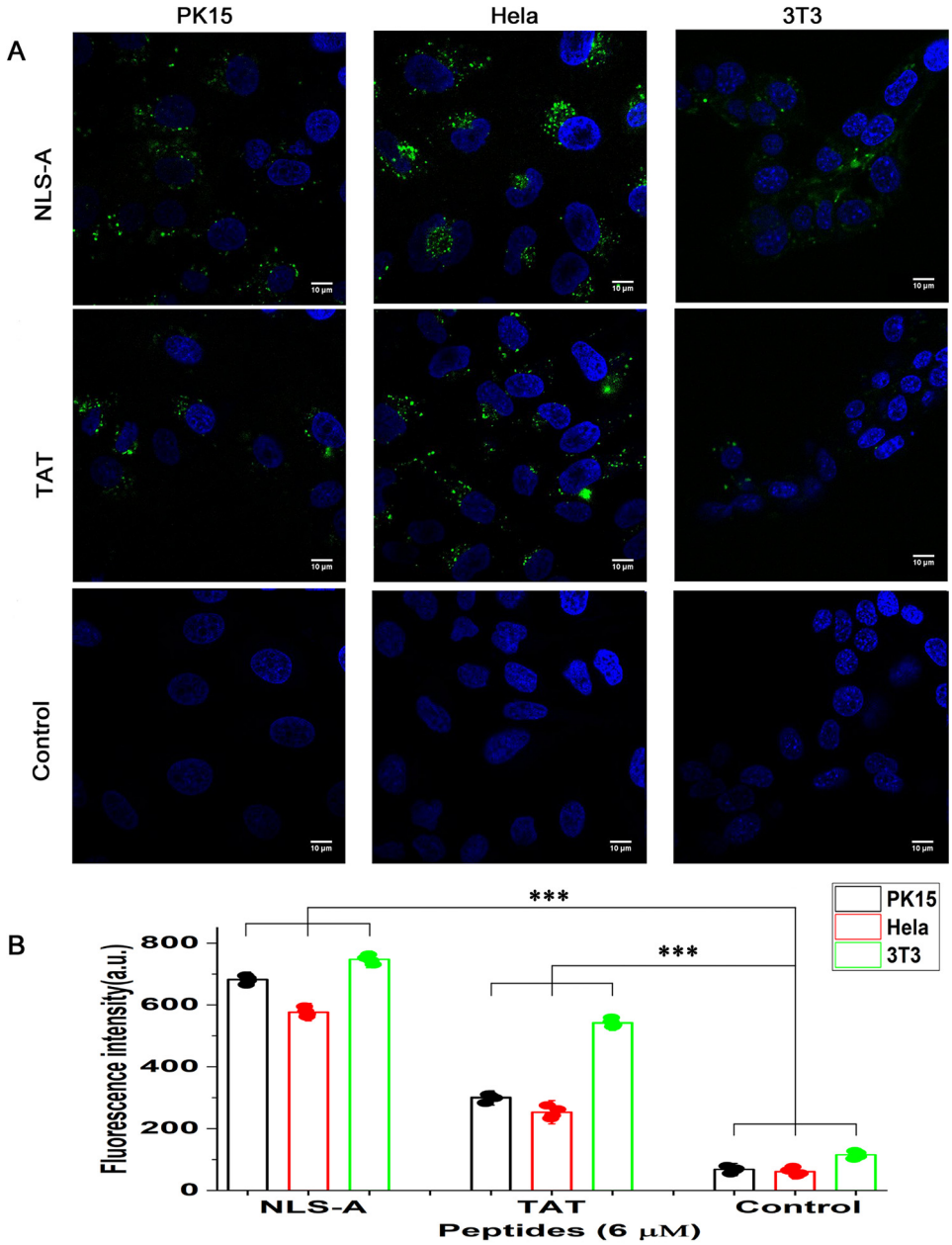

Figure 4. Cellular uptake of FITC-conjugated NLS-A and FITC-conjugated HIV-TAT. *A*, PK15, HeLa, and NIH3T3 cells were incubated with FITC-conjugated NLS-A (*upper row*) or FITC-conjugated HIV-TAT (*middle row*) for 30 min and washed three times with PBS before imaging with a dual-channel confocal laser-scanning microscope (Nikon TiE). A third test with buffer only was used as a treatment control (*bottom row*). *Green* indicates FITC signal in the cells, and cell nuclei (*blue*) are indicated by Hoechst. *B*, bar graph summarizing the fluorescence intensity of the PK15, HeLa, and NIH3T3 cells under the above three incubation treatments ($n = 4$; *error bars* represent S.D.; ***, $p < 0.001$). All *scale bars* represent 10 μm. *a.u.*, arbitrary units.

presence of NLS-A was significantly higher than that in the presence of FITC alone (Fig. 6*F*; $p < 0.001$). Therefore, a high concentration of NLS-A permeabilized the GUV membrane and caused a bidirectional flux of the dye across the membrane.

The NLS-A entered cells via endocytosis with multiple pathways

It appears that HIV TAT and other CPPs enter cells via endocytosis with distinct pathways (22). The punctate distribution of the NLS-A at low concentrations indicated that the peptide was translocated into cells via endocytosis. Dynamic tracking of NLS-A in live cells indicated that the NLS-A colocalized with Rab7–RFP in PK15 cells (Fig. 7*A*). Therefore, NLS-A was present in a late endosome after internalization. Next, we applied endocytosis inhibitors to cell cultures to further study the NLS-A entry mechanism. Inhibition of clathrin-mediated endocytosis (chlorpromazine) and macropinocytosis (*N*-(ethyl-*N*-isopropyl)-amiloride) and disruption of caveolae/lipid rafts (methyl-β-cyclodextrin) all dramatically decreased efficiency of NLS-A entry into cells (Fig. 7, *B* and *C*). Therefore, the three major endocytosis pathways were all involved in internalization of NLS-A at low concentration (6 μM). In addition, effects of F-actin on NLS-A internalization were also tested. Inhibition of actin polymerization by cytochalasin D dramatically decreased efficiency of NLS-A (6 μM) entry into PK15 cells

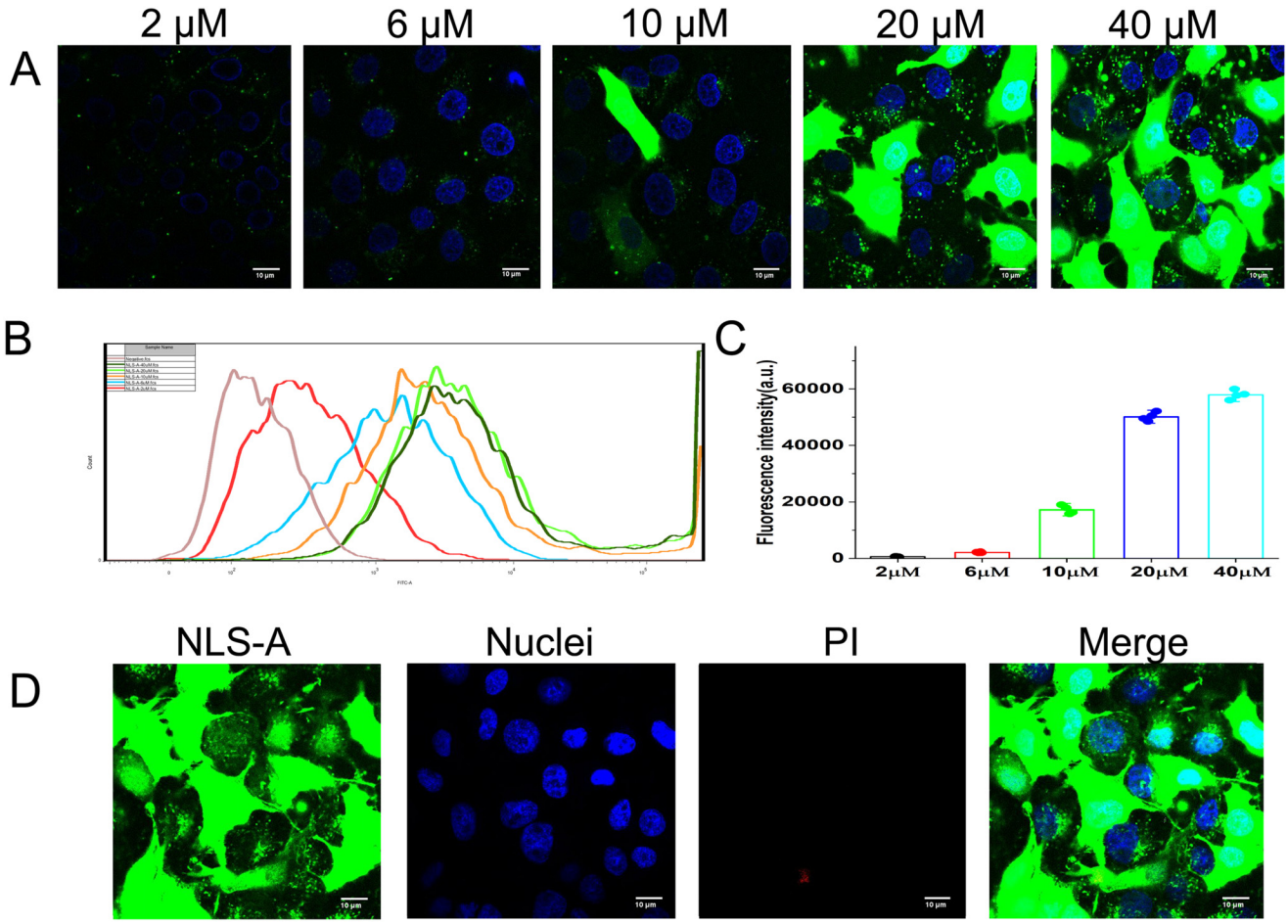

Figure 5. Cellular uptake of NLS-A is concentration-dependent. *A*, PK15 cells were incubated with serial concentrations of FITC-conjugated NLS-A (2, 6, 10, 20, and 40 μM) for 30 min at 37 °C and washed three times with PBS before imaging with a dual-channel confocal laser scanning microscope (Nikon TiE). *Green* indicates FITC signal in the cells, and cell nuclei (*blue*) are indicated by Hoechst. *B*, PK15 cells were incubated with serial concentrations of FITC-conjugated NLS-A (2, 6, 10, 20, and 40 μM) for 30 min at 37 °C. After the cells were trypsinized and washed, the cellular FITC fluorescence intensity of each treatment was analyzed by flow cytometry (BD FACSVerse). Flow cytometry results were processed by FlowJo software. *C*, bar graph summarizing the fluorescence intensity of the PK15 cells under the incubation treatments with the indicated NLS-A concentration ($n = 4$; *error bars* represent S.D.). *D*, PK15 cells under treatment of a high concentration of NLS-A (40 μM) were further stained by PI for viability test. All *scale bars* represent 10 μm. *a.u.*, arbitrary units.

(Fig. S4), which implicated F-actin to have a critical role in NLS-A internalization.

NLS-A had more efficient cellular uptake than HIV TAT

Finally, we compared the entry efficiency of NLS-A and HIV TAT. PK15 cells were incubated with FITC-conjugated NLS-A or HIV TAT at various concentrations, and cellular uptake efficiencies of the peptides were evaluated by flow cytometry. Mean fluorescence intensities were compared between NLS-A and HIV TAT at various concentrations, and NLS-A entry into PK15 cells was 10-fold more efficient than entry of HIV TAT in PK15 cells (Fig. 8). Similar results were also observed in HeLa cells (Fig. S5).

Discussion

In a mature PCV2 virion, viral genomic DNA is packaged by a capsid, assembled by 60 Cap subunits. The NLS of the PCV2 Cap is considered a critical element responsible for viral DNA packaging as the NLS, which is rich in positively charged residues, may interact with phosphate groups of viral DNA. Mutation of the NLS significantly decreases virus titers in cell culture (32, 33). In addition, based on a structural study, the NLS of the PCV2 Cap is apparently located around the 5-fold axis and buried inside the capsid (7). Perhaps NLSs from five neighboring PCV2 Caps at one icosahedral 5-fold axis of the capsid may be transiently externalized and penetrate cell membranes to release viral DNA into host cells (30). Regardless, in this study, NLS was capable of carrying foreign protein into various cells, and NLS-A had a cell penetration function similar to known CPPs, *e.g.* HIV TAT and polyarginine. Although NLS is located inside the capsid in a stable virion, it may externalize from the capsid to interact with the cell membranes when a capsid switches into a metastable state induced by factors from host cells during infection. In a previous study (31), five monoclonal antibodies were screened, and four were found to recognize an epitope (^{26}RPWLVHPRHRY^{36}) located in the NLS-B (Fig. 1, *A* and *C*); a similar epitope was reported by another group (34). We also screened a mAb against this epitope; it had a strong neutralization activity against PCV2 infection in cell culture (data not shown). Additionally, a well known and conserved CRAC motif was also identified in the NLS-B of the PCV2 Cap via fine mapping (Fig. 1). This motif was only present in the

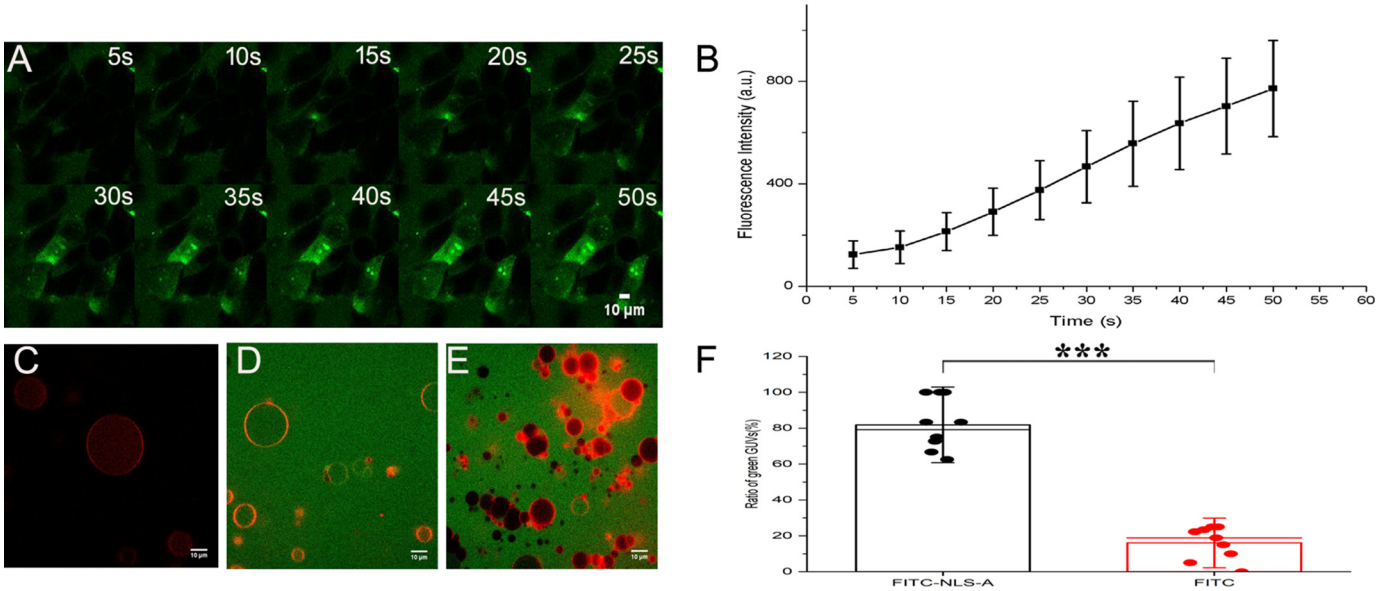

Figure 6. Rapid entry of the NLS-A into PK15 cells by penetrating the membranes. *A*, time lapse of NLS-A internalization after PK15 cells were treated with 40 μM peptide. Images were acquired at 5-s intervals. *Green* represents FITC-conjugated NLS-A in cells. *B*, bar graph summarizing the mean fluorescence intensity at each time point ($n = 100$; *error bars* represent S.D.) *C–F*, GUVs with encapsulated atto565 dye (*red*) in the absence of NLS-A (*C*) or the presence of the FITC-conjugated NLS-A (20 μM) (*D*). As a control, FITC alone (20 μM) was added into the GUV solution (*E*). *F*, ratios of GUVs containing FITC fluorescence (*green*). Data are represented as the mean ± S.D. (*error bars*) of 100 individual GUVs from 10 microscopic fields. ***, $p < 0.001$. Note that confocal images were collected after 1-h incubation of FITC-conjugated NLS-A, FITC alone, or buffer with GUV solutions, respectively. Membranes were visualized by DiI staining. All *scale bars* represent 10 μm. *a.u.*, arbitrary units.

NLS-B of the PCV2 Cap and not in PCV1 (Fig. 1*A*). Therefore, NLS externalization during PCV2 infection was possible, and the NLS-B may be involved in virus–host cell interactions via binding to cholesterol on membranes, although it does not function as a CPP (Fig. 3).

So far, the specific receptor(s) for PCV2 internalization has not been reported, although two glycosaminoglycans, namely heparan sulfate (HS) and chondroitin sulfate B, were identified as attachment receptors for PCV2 entry (35). Heparan sulfate proteoglycan (HSPG) is present on the outer leaflet of the plasma membrane via linkage of HS chains with distinct core proteins, such as syndecans and glypicans (36). Notably, there is accumulating evidence that HSPG may function as a cell-surface endocytosis receptor responsible for internalization of various macromolecular cargoes (37–39). It was reported that HS-mediated HIV TAT internalization is one of the crucial pathways of its cellular uptake (29, 40). Furthermore, HSPG-mediated endocytosis may exploit a distinct pathway, depending on the cellular context, ligand type, and HSPG isoform (*i.e.* syndecans or glypicans) (37). Recently, syndecan-4, a member of HSPGs, was reported to be a receptor for clathrin-mediated endocytosis (CME) of arginine-rich CPPs (38). Based on sequence mapping, the PCV2 Cap contained a putative heparin-binding motif (^{98}IRKVKV^{103}), although this motif was buried inside the capsid (7). Alternatively, the externalized, arginine-rich NLS of the PCV2 Cap may function as a binding motif responsible for interaction of PCV2 with HSPG on host cells and initiating endocytosis for PCV2 entry.

In studies of molecular mechanisms of PCV2 invading various swine cells, this virus exploited CME to infect a monocytic cell line, 3D4/31 (41). Surprisingly, blocking the CME pathway or inhibition of acidification of endosomes/lysosomes in epithelial cells significantly increased PCV2 infectivity (42, 43). Therefore, we inferred that PCV2 entry into epithelia cells via endocytosis was an invalid pathway for infection, or endocytosed PCV2 cannot successfully release its viral genome to a replication center to cause infection in epithelial cells. In general, endocytosed PCV2 in transport vesicles starts to fuse with early endosomes and will be targeted to an endolysosomal compartment. In this process, vesicles undergo acidification due to vacuolar-type ATPase pumping H^+ into vesicles. However, acidification of vesicles has an adverse effect on PCV2 infection of epithelia cells (43), indicating that viral DNA in a low-pH environment has a reduced chance of endosomal escape to finish the viral infection cycle. If the NLS-A can penetrate vesicle membranes and thereafter facilitate release of viral DNA into cytosol, its externalization from the capsid should be a key and rate-limiting step for endosomal escape of the viral genome. Clearly, acidification in transport vesicles will decrease the possibility of NLS externalization due to increased electrostatic repulsion between the low-pH environments (extra H^+) and the positively charged NLS. Therefore, increasing the acidity in transport vesicles will switch the equilibrium of the PCV2 capsid from a metastable (externalized NLS) toward a stable state (internalized NLS), whereas NLS externalization at various pH environments remains to be explored. In addition, in this study, NLS-A had an even distribution throughout cells with rapid entry when the extracellular concentration of the NLS-A was ≥10 μM (Figs. 5 and 6). Therefore, at high concentrations, NLS-A may directly penetrate cell membranes for internalization. Based on the 3D structure, NLS is located around the 5-fold axis of the capsid (7). Furthermore, a previous model also suggested that NLS might externalize through its 5-fold axis with the assistance of other surface loops around this area (30). If five NLSs simultaneously externalized through a 5-fold axis, they would form a five-NLS bundle with highly positively

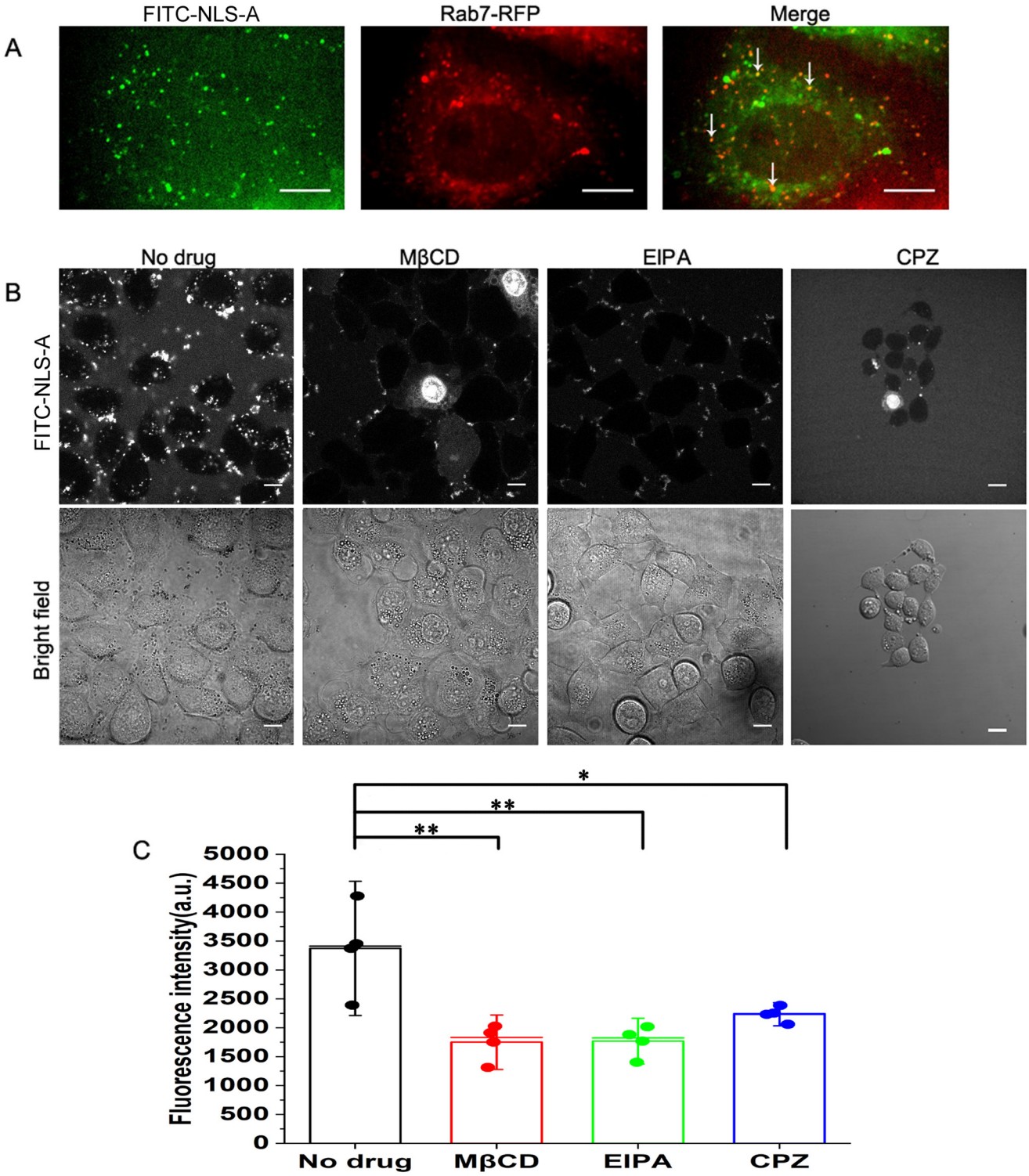

Figure 7. Cellular uptake of NLS-A via multiple endocytosis pathways. *A*, distributions of NLS-A (*left*) and Rab7 (*middle*) in PK15 cells. Colocalizations of NLS-A (6 μM) and Rab7 are indicated by *arrows* (*right*). *Scale bars*, 10 μm. *B*, effects of various inhibitors on cellular uptake of NLS-A (6 μM). Signals (*top panel*) indicate internalization of the NLS-A in PK15 cells. In the *bottom panel*, cells were examined with bright-field microscopy. *Scale bars*, 10 μm. *C*, mean fluorescence intensity per cell among four groups was analyzed by flow cytometry (*, $p < 0.05$; **, $p < 0.01$; *error bars* represent S.D.). *a.u.*, arbitrary units; *CPZ*, chlorpromazine; *EIPA*, *N*-(ethyl-*N*-isopropyl)-amiloride; *MβCD*, methyl-β-cyclodextrin.

charged residues. Therefore, this bundle should be more efficient to penetrate the cell membrane than one NLS because it is present a higher concentration (>4 mM) at the local membrane. Previous experiments also suggested that CPPs in tandem were more likely to penetrate cell membranes (27).

In our study, cellular uptake of the NLS-A was superior to that of HIV TAT (Fig. 8 and Fig. S5), the most popular CPP for use in applications. Sequence comparison revealed that NLS-A contains 2 more arginines and 1 more phenylalanine/tyrosine residue than HIV TAT (Fig. 1). Efficiency of peptide-penetrat-

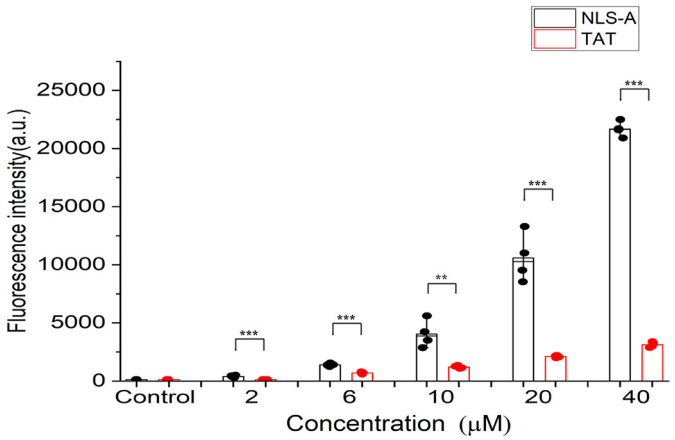

Figure 8. Cellular uptake of NLS-A is more efficient than HIV TAT at various concentrations. PK15 cells were incubated with increasing concentrations of NLS-A or HIV TAT (*x axis*) at 37 °C for 30 min and subjected to flow cytometry analysis. The *y axis* represents the average fluorescence intensity per group. Data are represented as the mean ± S.D. (*error bars*) of four independent experiments (**, $p < 0.01$; ***, $p < 0.001$). *a.u.*, arbitrary units.

ing biological membranes is correlated with numbers of arginine and hydrophobic residues (44, 45). A negative Gaussian membrane curvature, topologically required for pore formation (46), is maximized when there are ~9 polyarginines in the peptide (45). Interestingly, the NLS-A also contains 9 arginine residues, despite being interrupted by 3 noncharged residues, with 1 tyrosine residue (Tyr^3) and 1 phenylalanine residue (Phe^8) interspersed in this peptide (Fig. 1). The aromatic side chains of tyrosine and phenylalanine may insert into and anchor NLS-A on membranes. It was suggested that decreasing arginine residues in most CPPs is compensated by simultaneous increases in lysine and hydrophobic content (45). Notably, insertion of a bulky aromatic ring of phenylalanine (Phe) or tyrosine (Tyr) into membranes apparently requires some degree of accommodation, thereby favoring bending of the membrane into a positive curvature whereby a single hydrophobic residue can dramatically affect translocation of CPPs (45). However, contributions of both Phe and Tyr and effects of their positions (or distance) along the NLS of the PCV2 Cap to their cell-penetration capacity remain to be determined. Altogether, due to its powerful cell-penetrating ability, the NLS-A may not only have a critical role in viral DNA release into the cytoplasm by overcoming membrane barriers, but it may also be one of best future shuttles for *in vivo* drug delivery.

Materials and methods

Cells and reagents

PK15 cells (obtained from Xiaoming Yuan, Nanjing Agricultural University), HeLa S6 cells, and NIH3T3 cells (from Cell Bank, Shanghai Institutes for Biological Sciences, Chinese Academy of Sciences, Shanghai, China) were maintained in Dulbecco's modified Eagle's medium (high glucose with L-glutamine) (Life Technologies) containing 10% fetal bovine serum (Life Technologies), 100 units/ml penicillin, and 100 μg/ml streptomycin (Life Technologies) at 37 °C in a 5% CO_2 incubator and passaged every 2–3 days. *Spodoptera frugiperda* (Sf9) cells were purchased from Life Technologies and maintained in Sf-900™ II serum-free medium (Life Technologies) for suspension culture at 27 °C. Cells were subcultured when cell density reached 3.0×10^6 cells/ml. Cytochalasin D, Hoechst 33342, and PI were also purchased from Life Technologies. All chemicals, unless otherwise stated, were purchased from Sigma-Aldrich.

Protein expression, purification, and cellular uptake

Gene fragments containing *nls–egfp* and *egfp* were subcloned into protein expression vector pET100/D-TOPO (Life Technologies), respectively. Recombinant plasmids were analyzed by DNA sequencing for double strands to confirm that no mutation was introduced in both clones, and then correct plasmids were transformed into BL21(DE3) competent cells (TransGen, Beijing, China) for protein expression. When the A_{600} of the *Escherichia coli* culture reached 0.8–1.0, proteins of interest (NLS–EGFP and EGFP) were expressed by adding 1 mM isopropyl thiogalactopyranoside to the culture for 3 h at 37 °C. Finally, cells were harvested by centrifugation at 9,000 × *g* for 10 min at 4 °C and stored at −80 °C for use. For protein purification, a cell pellet harvested from 250 ml of BL21 *E. coli* culture was suspended in 25 ml of buffer A (0.1 M NaH_2PO_4, 0.1 M Na_2HPO_4, 20 mM imidazole, 10 mM Tris base, 300 mM NaCl, and 5% glycerol, pH 8.0) with 0.5% Triton X-100, 5 mM β-mercaptoethanol, and protease inhibitors (0.1 mM PMSF and 1 unit of leupeptin/ml), then cells were disrupted by sonication, and the homogenate was cleared by centrifugation (15,000 × *g*, 20 min). The supernatant was loaded on a prepacked HisTrap™ HP column (GE Healthcare) attached to an FPLC instrument (ÄKTA, GE Healthcare). After the column was washed with 10 ml of buffer A, the protein of interest was eluted with 10 ml of buffer B (300 mM imidazole and 300 mM NaCl, pH 7.0), and fractions (1 ml) were collected. Purity was assessed with SDS-PAGE, and protein was dialyzed twice in phosphate-buffered saline (PBS). Protein concentration was quantified using a BCA protein assay kit (Sangon Biotech, Shanghai, China) after which purified NLS–EGFP or EGFP (4 μg/ml) was incubated with PK15 or Sf9 cells in 35-mm glass-bottomed Petri dishes (Beijing Solarbio Science and Technology Co., Ltd., Beijing, China) for 1 h. Finally, cells were washed three times with PBS to removed unbound proteins and then imaged by confocal microscopy.

Peptide synthesis, labeling, and cellular uptake

Peptides of NLS-A (MTYPRRRFRRRRHRPRS), NLS-B (QILRRRPWLVHPRHRYRWRRK), and HIV TAT protein transduction domain (YGRKKRRQRRR) were synthesized by GenScript, Inc. (Nanjing, China). All peptides were conjugated with FITC at the NH_2-terminal ends, and further purified via HPLC (>95%). The lyophilized peptides were stored at −80 °C before use. For cellular uptake assays, each peptide was first dissolved in aseptic water as a stock solution (2 mg/ml) and then added to cell cultures at various concentrations. After incubations, cells were washed three times with PBS to removed unbound peptides. Live images were acquired by confocal microscopy.

Cells treated with inhibitors

Cells were pretreated with various inhibitors in respective media for 30 min at 37 °C. Then the medium was replaced with fresh medium containing the NLS-A peptide as well as corre-

sponding inhibitors. After 30 min of incubation at 37 °C, cells were washed twice with fresh medium and analyzed by fluorescence microscopy or flow cytometry. Work concentrations of inhibitors were 10 μM for cytochalasin D, 10 μg/ml for chlorpromazine, 5 mM for methyl-β-cyclodextrin, and 50 μM for *N*-(ethyl-*N*-isopropyl)-amiloride in media.

Preparation of GUVs

The lipids 1,2-diphytanoyl-*sn*-glycero-3-phosphocholine and 1,2-dioleoyl-*sn*-glycero-3-phosphocholine were purchased from Avanti Polar Lipids, Inc. (Alabaster, AL) and used without further preparation. The GUVs with encapsulated atto565 dye (Invitrogen) were prepared using electroformation and labeled with DiI (1,1″-dioctadecyl-3,3,3″,3″-tetramethylindocarbocyanine perchlorate; Invitrogen) to illustrate the border. Lipid mixtures in chloroform were deposited and desiccated on indium tin oxide–coated glass slides before swelling with sorbitol (100 mM) solution containing atto565 under a 10-Hz alternating current electric field. After 128 min, the sorbitol solution containing GUVs, which was diluted in PBS, pH 7.4, was collected, and GUVs were detected under a laser-scanning confocal microscope.

Flow cytometry

Cells were seeded on 6-well plates at a density of 1.0×10^6 cells/well and then incubated with FITC-conjugated NLS-A, NLS-B, and HIV TAT peptides at various concentrations or purified proteins (NLS–EGFP or EGFP) in fresh Opti-MEM (Life Technologies), respectively, for 30 min or 1 h at 37 °C. After incubation, cells were washed with PBS and detached by 0.25% trypsin (Life Technologies) at 37 °C for 2 min. Finally, Dulbecco's modified Eagle's medium containing 10% fetal bovine serum was added to terminate trypsinization. Then cells were washed three times with PBS and finally resuspended in PBS before flow cytometry analysis (BD FACSVerse, BD Biosciences). Vital cells were gated based on sideward and forward scatter. In each sample, 10,000 cells were collected, and arbitrary fluorescence intensity of each cell was acquired.

Confocal laser-scanning microscopy

For detection of cellular uptake of peptides, cells were seeded on 35-mm glass-bottomed Petri dishes at a density of 5×10^5 cells/well and then incubated with Opti-MEM containing peptides at the indicated concentrations (2, 6, 10, 20, and 40 μM) for 30 min at 37 °C. Thereafter, cells were washed twice with PBS and cultured with fresh medium without phenol red. Before imaging, Hoechst 33342 was added (10 μM final concentration in medium). Confocal images were collected with an inverted Nikon TiE microscope attached to a Confocal C2 system (Nikon, Japan) with an EMCCD camera (Andor iXon Ultra897). The FITC and Hoechst were excited with 488 and 405 nm lasers, respectively. For detection of colocalization of NLS-A and endosomes, cells were first transfected with Rab7–RFP plasmid (obtained from Yang Liu, Chinese Academy of Sciences). At 24 h after transfection, cells were incubated with 6 μM NLS-A for 30 min at 37 °C. Then cells were washed twice with PBS and cultured with fresh medium without phenol red. Finally, live images of the cells were collected by an inverted Nikon TiE microscope connected to an UltraVIEW VOX system spinning disc (PerkinElmer Life Sciences) with an EMCCD camera (C9100-13, Hamamatasu). The microscope was equipped with a heated stage maintained at 37 °C and 5% CO_2. FITC and RFP were excited with 488 and 561 nm lasers, respectively. For detection of membrane permeability, 10 μl of GUVs with encapsulated atto565 dye suspension were first diluted in 1 ml of PBS, pH 7.4, and labeled with DiI (1 μM), and then the suspension was incubated with FITC–NLS-A (20 μM), FITC dye alone (20 μM), or PBS, respectively, for 1 h at room temperature. After incubation, the mixture was poured into a 35-mm glass-bottomed Petri dish and placed on an inverted Nikon TiE microscope attached to a Confocal C2 system with an EMCCD camera (Andor iXon Ultra897). A 488 nm laser was used to excite FITC, whereas a 561 nm laser was used to excite atto565 and DiI.

Statistical analyses

For flow cytometry, mean fluorescence intensity and the percentage of cells with intracellular fluorescence were analyzed for each group with FlowJo software (BD Biosciences). For confocal images, mean fluorescence intensity of each cell and GUV was measured and processed by ImageJ software (National Institutes of Health, Bethesda, MD). All statistical analyses were performed using SPSS software (Version 16, SPSS, Inc., Chicago, IL). Differences were considered significant for $p < 0.05$ (*), $p < 0.01$ (**), and $p < 0.001$ (***).

Author contributions—W. Y., B. X., and Y. Y. conceptualization; W. Y., Y. Z., Y. D., Y. W., P. J., Y. S., and Y. Y. resources; W. Y., Y. Z., B. X., Y. W., A. W., Y. S., and Y. Y. data curation; W. Y., Y. Z., B. X., Y. W., and Y. Y. formal analysis; W. Y., Y. Z., Y. S., and Y. Y. validation; W. Y., Y. Z., Y. S., and Y. Y. visualization; W. Y., B. X., Y. D., Y. W., P. J., Y. S., and Y. Y. methodology; W. Y., A. W., Y. S., and Y. Y. writing-original draft; W. Y., Y. Z., B. X., A. W., Y. S., and Y. Y. writing-review and editing; Y. Z., B. X., Y. D., P. J., Y. S., and Y. Y. investigation; A. W., Y. S., and Y. Y. supervision; A. W. and Y. Y. funding acquisition; A. W., Y. S., and Y. Y. project administration; Y. S. software.

References

1. Tischer, I., Gelderblom, H., Vettermann, W., and Koch, M. A. (1982) A very small porcine virus with circular single-stranded DNA. *Nature* **295,** 64–66 CrossRef Medline
2. Segalés, J., Kekarainen, T., and Cortey, M. (2013) The natural history of porcine circovirus type 2: from an inoffensive virus to a devastating swine disease? *Vet. Microbiol.* **165,** 13–20 CrossRef Medline
3. Tischer, I., Rasch, R., and Tochtermann, G. (1974) Characterization of papovavirus-and picornavirus-like particles in permanent pig kidney cell lines. *Zentralbl. Bakteriol. Orig. A* **226,** 153–167 Medline
4. Palinski, R., Piñeyro, P., Shang, P., Yuan, F., Guo, R., Fang, Y., Byers, E., and Hause, B. M. (2017) A novel porcine circovirus distantly related to known circoviruses is associated with porcine dermatitis and nephropathy syndrome and reproductive failure. *J. Virol.* **91,** e01879-16 CrossRef Medline
5. Phan, T. G., Giannitti, F., Rossow, S., Marthaler, D., Knutson, T. P., Li, L., Deng, X., Resende, T., Vannucci, F., and Delwart, E. (2016) Detection of a novel circovirus PCV3 in pigs with cardiac and multi-systemic inflammation. *Virol. J.* **13,** 184 CrossRef Medline
6. Liu, Q., Tikoo, S. K., and Babiuk, L. A. (2001) Nuclear localization of the ORF2 protein encoded by porcine circovirus type 2. *Virology* **285,** 91–99 CrossRef Medline
7. Khayat, R., Brunn, N., Speir, J. A., Hardham, J. M., Ankenbauer, R. G., Schneemann, A., and Johnson, J. E. (2011) The 2.3-angstrom structure of porcine circovirus 2. *J. Virol.* **85,** 7856–7862 CrossRef Medline

8. Wagstaff, K. M., and Jans, D. A. (2007) Nucleocytoplasmic transport of DNA: enhancing non-viral gene transfer. *Biochem. J.* **406,** 185–202 CrossRef Medline
9. Douglas, J. L., and Quinlan, M. P. (1994) Efficient nuclear localization of the Ad5 E1A 12S protein is necessary for immortalization but not cotransformation of primary epithelial cells. *Cell Growth Differ.* **5,** 475–483 Medline
10. Futaki, S. (2005) Membrane-permeable arginine-rich peptides and the translocation mechanisms. *Adv. Drug Deliv. Rev.* **57,** 547–558 CrossRef Medline
11. Frankel, A. D., and Pabo, C. O. (1988) Cellular uptake of the tat protein from human immunodeficiency virus. *Cell* **55,** 1189–1193 CrossRef Medline
12. Vivès, E., Brodin, P., and Lebleu, B. (1997) A truncated HIV-1 Tat protein basic domain rapidly translocates through the plasma membrane and accumulates in the cell nucleus. *J. Biol. Chem.* **272,** 16010–16017 CrossRef Medline
13. Derossi, D., Joliot, A. H., Chassaing, G., and Prochiantz, A. (1994) The third helix of the antennapedia homeodomain translocates through biological membranes. *J. Biol. Chem.* **269,** 10444–10450 Medline
14. Jones, A. T., and Sayers, E. J. (2012) Cell entry of cell penetrating peptides: tales of tails wagging dogs. *J. Control. Release* **161,** 582–591 CrossRef Medline
15. Rapoport, M., and Lorberboum-Galski, H. (2009) TAT-based drug delivery system—new directions in protein delivery for new hopes? *Expert Opin. Drug Deliv.* **6,** 453–463 CrossRef Medline
16. Chen, B., Liu, Q., Zhang, Y., Xu, L., and Fang, X. (2008) Transmembrane delivery of the cell-penetrating peptide conjugated semiconductor quantum dots. *Langmuir* **24,** 11866–11871 CrossRef Medline
17. Ruan, G., Agrawal, A., Marcus, A. I., and Nie, S. (2007) Imaging and tracking of tat peptide-conjugated quantum dots in living cells: new insights into nanoparticle uptake, intracellular transport, and vesicle shedding. *J. Am. Chem. Soc.* **129,** 14759–14766 CrossRef Medline
18. Abes, R., Arzumanov, A. A., Moulton, H. M., Abes, S., Ivanova, G. D., Iversen, P. L., Gait, M. J., and Lebleu, B. (2007) Cell-penetrating-peptide-based delivery of oligonucleotides: an overview. *Biochem. Soc. Trans.* **35,** 775–779 CrossRef Medline
19. Cleal, K., He, L., Watson, P. D., and Jones, A. T. (2013) Endocytosis, intracellular traffic and fate of cell penetrating peptide based conjugates and nanoparticles. *Curr. Pharm. Des.* **19,** 2878–2894 CrossRef Medline
20. Reissmann, S. (2014) Cell penetration: scope and limitations by the application of cell-penetrating peptides. *J. Pept. Sci.* **20,** 760–784 CrossRef Medline
21. Jones, S. W., Christison, R., Bundell, K., Voyce, C. J., Brockbank, S. M., Newham, P., and Lindsay, M. A. (2005) Characterisation of cell-penetrating peptide-mediated peptide delivery. *Br. J. Pharmacol.* **145,** 1093–1102 CrossRef Medline
22. Duchardt, F., Fotin-Mleczek, M., Schwarz, H., Fischer, R., and Brock, R. (2007) A comprehensive model for the cellular uptake of cationic cell-penetrating peptides. *Traffic* **8,** 848–866 CrossRef Medline
23. Koren, E., and Torchilin, V. P. (2012) Cell-penetrating peptides: breaking through to the other side. *Trends Mol. Med.* **18,** 385–393 CrossRef Medline
24. Brock, R. (2014) The uptake of arginine-rich cell-penetrating peptides: putting the puzzle together. *Bioconjug. Chem.* **25,** 863–868 CrossRef Medline
25. Nakase, I., Hirose, H., Tanaka, G., Tadokoro, A., Kobayashi, S., Takeuchi, T., and Futaki, S. (2009) Cell-surface accumulation of flock house virus-derived peptide leads to efficient internalization via macropinocytosis. *Mol. Ther.* **17,** 1868–1876 CrossRef Medline
26. Kaplan, I. M., Wadia, J. S., and Dowdy, S. F. (2005) Cationic TAT peptide transduction domain enters cells by macropinocytosis. *J. Control. Release* **102,** 247–253 CrossRef Medline
27. Erazo-Oliveras, A., Najjar, K., Dayani, L., Wang, T. Y., Johnson, G. A., and Pellois, J. P. (2014) Protein delivery into live cells by incubation with an endosomolytic agent. *Nat. Methods* **11,** 861–867 CrossRef Medline
28. Wadia, J. S., Stan, R. V., and Dowdy, S. F. (2004) Transducible TAT-HA fusogenic peptide enhances escape of TAT-fusion proteins after lipid raft macropinocytosis. *Nat. Med.* **10,** 310–315 CrossRef Medline
29. Melikov, K., and Chernomordik, L. V. (2005) Arginine-rich cell penetrating peptides: from endosomal uptake to nuclear delivery. *Cell. Mol. Life Sci.* **62,** 2739–2749 CrossRef Medline
30. Wang, N., Zhan, Y., Wang, A., Zhang, L., Khayat, R., and Yang, Y. (2016) *In silico* Analysis of surface structure variation of PCV2 capsid resulted from loops mutation of its capsid protein (Cap). *J. Gen. Virol.* **97,** 3331–3344 CrossRef Medline
31. Levitan, I., Singh, D. K., and Rosenhouse-Dantsker, A. (2014) Cholesterol binding to ion channels. *Front. Physiol.* **5,** 65 CrossRef Medline
32. Shuai, J., Fu, L., Zhang, X., Zhu, B., Li, X., He, Y., and Fang, W. (2011) Functional exchangeability of the nuclear localization signal (NLS) of capsid protein between PCV1 and PCV2 *in vitro*: implications for the role of NLS in viral replication. *Virol. J.* **8,** 341 CrossRef Medline
33. Beach, N. M., Smith, S. M., Ramamoorthy, S., and Meng, X. J. (2011) Chimeric porcine circoviruses (PCV) containing amino acid epitope tags in the C terminus of the capsid gene are infectious and elicit both anti-epitope tag antibodies and anti-PCV type 2 neutralizing antibodies in pigs. *J. Virol.* **85,** 4591–4595 CrossRef Medline
34. Mahé, D., Blanchard, P., Truong, C., Arnauld, C., Le Cann, P., Cariolet, R., Madec, F., Albina, E., and Jestin, A. (2000) Differential recognition of ORF2 protein from type 1 and type 2 porcine circoviruses and identification of immunorelevant epitopes. *J. Gen. Virol.* **81,** 1815–1824 CrossRef Medline
35. Misinzo, G., Delputte, P. L., Meerts, P., Lefebvre, D. J., and Nauwynck, H. J. (2006) Porcine circovirus 2 uses heparan sulfate and chondroitin sulfate B glycosaminoglycans as receptors for its attachment to host cells. *J. Virol.* **80,** 3487–3494 CrossRef Medline
36. Bishop, J. R., Schuksz, M., and Esko, J. D. (2007) Heparan sulphate proteoglycans fine-tune mammalian physiology. *Nature* **446,** 1030–1037 CrossRef Medline
37. Christianson, H. C., and Belting, M. (2014) Heparan sulfate proteoglycan as a cell-surface endocytosis receptor. *Matrix Biol.* **35,** 51–55 CrossRef Medline
38. Kawaguchi, Y., Takeuchi, T., Kuwata, K., Chiba, J., Hatanaka, Y., Nakase, I., and Futaki, S. (2016) Syndecan-4 is a receptor for clathrin-mediated endocytosis of arginine-rich cell-penetrating peptides. *Bioconjug. Chem.* **27,** 1119–1130 CrossRef Medline
39. Wittrup, A., Zhang, S. H., ten Dam, G. B., van Kuppevelt, T. H., Bengtson, P., Johansson, M., Welch, J., Mörgelin, M., and Belting, M. (2009) ScFv antibody-induced translocation of cell-surface heparan sulfate proteoglycan to endocytic vesicles: evidence for heparan sulfate epitope specificity and role of both syndecan and glypican. *J. Biol. Chem.* **284,** 32959–32967 CrossRef Medline
40. Richard, J. P., Melikov, K., Brooks, H., Prevot, P., Lebleu, B., and Chernomordik, L. V. (2005) Cellular uptake of unconjugated TAT peptide involves clathrin-dependent endocytosis and heparan sulfate receptors. *J. Biol. Chem.* **280,** 15300–15306 CrossRef Medline
41. Misinzo, G., Meerts, P., Bublot, M., Mast, J., Weingartl, H. M., and Nauwynck, H. J. (2005) Binding and entry characteristics of porcine circovirus 2 in cells of the porcine monocytic line 3D4/31. *J. Gen. Virol.* **86,** 2057–2068 CrossRef Medline
42. Misinzo, G., Delputte, P. L., Lefebvre, D. J., and Nauwynck, H. J. (2009) Porcine circovirus 2 infection of epithelial cells is clathrin-, caveolae- and dynamin-independent, actin and Rho-GTPase-mediated, and enhanced by cholesterol depletion. *Virus Res.* **139,** 1–9 CrossRef Medline
43. Misinzo, G., Delputte, P. L., and Nauwynck, H. J. (2008) Inhibition of endosome-lysosome system acidification enhances porcine circovirus 2 infection of porcine epithelial cells. *J. Virol.* **82,** 1128–1135 CrossRef Medline
44. Najjar, K., Erazo-Oliveras, A., Mosior, J. W., Whitlock, M. J., Rostane, I., Cinclair, J. M., and Pellois, J. P. (2017) Unlocking endosomal entrapment with supercharged arginine-rich peptides. *Bioconjug. Chem.* **28,** 2932–2941 CrossRef Medline
45. Mishra, A., Lai, G. H., Schmidt, N. W., Sun, V. Z., Rodriguez, A. R., Tong, R., Tang, L., Cheng, J., Deming, T. J., Kamei, D. T., and Wong, G. C. (2011) Translocation of HIV TAT peptide and analogues induced by multiplexed membrane and cytoskeletal interactions. *Proc. Natl. Acad. Sci. U.S.A.* **108,** 16883–16888 CrossRef Medline
46. Mishra, A., Gordon, V. D., Yang, L., Coridan, R., and Wong, G. C. (2008) HIV TAT forms pores in membranes by inducing saddle-splay curvature: potential role of bidentate hydrogen bonding. *Angew. Chem.* **47,** 2986–2989 CrossRef Medline